

# Low Crustal Fluid Reservoirs in Ultramafic Cumulates of Kamchatka

A. G. Simakin<sup>a</sup>, \* and O. Yu. Shaposhikova<sup>a</sup>

<sup>a</sup> *Korzhinskii Institute of Experimental Mineralogy, Russian Academy of Sciences, Chernogolovka, Russia*

\**e-mail: simakin@iem.ac.ru*

Received March 16, 2022; revised May 25, 2022; accepted June 17, 2023

**Abstract**—Based on published geophysical and petrological data, lower crustal fluid reservoirs have been proposed below the Klyuchevskoy Volcano, expressed as a low  $V_p/V_s$  anomaly. A high  $V_p/V_s$  anomaly under the proposed fluid reservoir is interpreted as a zone of magma accumulation. The localization of fluids in these reservoirs in the ductile lower crust can vary from isolated inclusions to filling of microfractures over a time scale of several months. Using a simplified poroelastic model, it is shown that the transition in the topology of pore space filled with fluid or melt can provide the observed changes in  $V_p/V_s$  in the anomalies of high and low values at a melt content of several vol % and fluid content less than 1 vol %, respectively. In zones of active volcanism, such as the Klyuchevskaya group of volcanoes (KGV), fluid reservoirs are localized in ultramafic cumulates formed during the early high-temperature stage of magma fractionation. Ultramafic xenoliths in the products of eruptions of the KGV and Avachinsky volcanoes, often interpreted as mantle rocks, formed at pressures of about 5 kbar or depths of about 18–20 km in accordance with two-pyroxene geo-thermobarometry and the content of volatiles in melt inclusions in olivine and spinel. When crossing by ascending magmas, the fluid-containing reservoir experiences mechanical failure and injects a certain amount of fluid into the magma, which then captures pieces of crushed magmatic cumulates. The composition of melt inclusions in olivine can reveal records of the magma-fluid interaction.

**Keywords:** deep crustal fluid reservoirs, poro-elasticity, geo-barometry, xenoliths, brittle-ductile transition, Kamchatka, Klyuchevskoy Group Volcanoes

**DOI:** 10.1134/S0869591123060036

## INTRODUCTION

In the continental crust, the fluid components (mostly H<sub>2</sub>O and CO<sub>2</sub>) are an important agent enabling melting (Li et al., 2022) and affecting both metasomatism and metamorphism (Putins and Austrheim, 2010). Devolatilization of subducted crustal rocks creates large fluxes of H<sub>2</sub>O and CO<sub>2</sub> at active continental margins (Bekaert et al., 2021). The released fluids play an essential role in the formation of magma and in controlling the rheology of the rock mass in the mantle wedge (Hirth and Kohlstedt, 2013). The fluids, crossing and modifying mantle wedge, reach the crust of the overriding plate and mainly return to the Earth's surface. The recycling of volatiles in subduction zones is attributed predominantly to volcanoes due to transport by erupting magmas and passive degassing. For CO<sub>2</sub>, which is easier to track and is a more important component of the fluid than water for global warming, it has been estimated from measurements (not extrapolated to the entire globe) that volcanic activity releases about 66.4 Mt/yr of CO<sub>2</sub>, while tectonic, hydrothermal, and inactive volcanic areas—about 66 Mt/yr (Burton and Sawyer, 2013). According to some estimates based on petrological observations of the distribution of quartz veins,

the total mass flow of water fluid through the rocks of a volcanically inactive accretionary prism can reach 10<sup>5</sup> m<sup>3</sup>/m<sup>2</sup> (Breeding and Ague, 2002). These estimates suggest that large volumes of fluid may accumulate in deep crust before they cross the brittle upper crust in tectonically active areas. However, little is known about the state and dynamics of fluids in the lower crust of the active subduction zones.

Exploited fluid reservoirs, including oil and gas fields and geothermal systems, are localized in the brittle upper crust in hydraulically connected porous and fractured rocks. The behavior of fluid in the ductile lower crust cannot be directly observed and is the subject of debate. As a rule, fluid pressure passes from the hydrostatic level to the lithostatic level below the brittle-ductile rheological boundary (Zencher et al., 2006). In addition to mechanical factors, in regulating the composition, pressure and dynamics of fluids in the lower layers of the Earth's crust, the interaction of fluids with rocks is of great importance, which is studied exclusively by petrologists on samples of metamorphic rocks representing fossil deep crustal reservoirs. During retrograde metamorphism, volatiles can be consumed by dry rocks (for example, granulites), thereby reducing the volume of fluids and the activity of H<sub>2</sub>O and CO<sub>2</sub> and forming concentrated brines

(e.g., Markl and Bucher, 1998; Safonov et al., 2019) at a pressure much lower than hydrostatic (Yardley and Valley, 1997). On the contrary, with progressive metamorphism, fluid and porosity are generated during devolatilization (thermal decomposition of carbonates and hydrosilicates) (Yardley, 2009). A general theory of the transport of fluid released at the progressive stage of metamorphism has been developed (Connolly and Podladchikov, 2013). It is shown that ductile rocks are compacted, and light fluid migrates upwards in the form of porosity waves. The typical length scale of the compaction wave for the dehydration of amphibolites in the low crust is 31 m, the time scale is 10 Ky, which corresponds to the geodynamic events of several Mys.

At active continental margins, high fluid flux from a subducting slab can cause the formation of renewable deep fluid reservoirs in the lower crust. Permanent tectonic deformations, thermal stresses and hydraulic shocks caused by periodic magma intrusions lead to the formation and healing of cracks on time scales much shorter than the compaction time. As a result of healing, open fractures transform into weakly connected pores (including fluid inclusions in minerals). The transport of fluids from mantle-derived basalts to the base of the crust can be illustrated by observations of mantle and lower crust granulite xenoliths from Neogene alkaline basalts in the Pannonian Basin. Volcanism in the Pannonian Basin is associated with subduction (extensional regime due to slab roll back (Horváth et al., 2015)). Granulitic xenoliths contain reduced CO<sub>2</sub>–CO fluid (about 10 mol % of CO) as inclusions in minerals (Torok et al., 2005). Xenoliths of the upper mantle, mainly spinel lherzolites, in the same locality also contain fluid inclusions of CO<sub>2</sub>–CO in *Cpx*, *Opx* and bubbles in melt pockets with a total volume of up to 20 vol % (Créon et al., 2016). The average content of CO<sub>2</sub> fluid in the lithospheric mantle at the Moho depth was estimated at about 2000 ppm or 0.5–0.6 vol % (at a fluid density of about 1 g/cm<sup>3</sup> at a rock density of 3 g/cm<sup>3</sup>). Thus, 8–2 Mys ago, granulites in the Pannonian basin were fluxed with CO<sub>2</sub> transported by alkaline basalts.

Active subduction and related volcanism in Kamchatka make it possible to study in real time the state of fluid and the processes of fluid-rock, fluid-magma interaction in the low crust. In this paper, we analyze the published geophysical data and the results of petrological studies of the mafic xenoliths of the Klyuchevskaya group of volcanoes and Avachinsky volcano, which provide information on the behavior of deep crustal fluids.

#### SEISMIC DATA ON THE STATE OF DEEP FLUID IN SUBDUCTION ZONE

The fluid, even at a realistically small volume contents (several vol %), has a strong influence on the

velocity of the seismic waves propagation. Starting from the classical works (Berryman, 1995), many models of the mechanical properties of porous rocks have recently been developed, especially in the application of seismic methods in oil and natural gas exploration (for example, Guo et al., 2021 and references therein). There are models including effect of dual-pores filled with two-phase fluids (e.g., Ba et al., 2017). However, these theoretical models, which demonstrate the solution of complex equations, cannot give simple estimates of the specific effects on seismic velocities  $V_p$  and  $V_s$  associated with deep crustal fluid reservoirs. Under high *P-T* conditions, the solid matrix easily dissolves in the fluid, which ensures a rapid change in the structure of the pore space, including rapid healing of cracks and recrystallization. In addition, melt has a compressibility close to that of the crystalline matrix and significantly lower than the fluid compressibility. Below, for clarity, a simplified model is derived, aimed at predicting the change in mechanical properties during the transition of fluid and melt localization from cracks to inclusions.

#### Model

In isotropic rock, seismic velocities are proportional to the square root of the corresponding Lamé mechanical parameters:

$$V_s = (\mu/\rho)^{1/2} \text{ and } V_p = ((2\mu + \lambda)/\rho)^{1/2} \quad (1) \\ = (K(1 + 4/3\gamma)/\rho)^{1/2},$$

where  $\mu = G$  and  $K$  are shear and bulk moduli, respectively,  $\nu$  is Poisson's ratio and  $\gamma = G/K = 3(1 - 2\nu)/2(1 + \nu)$ . These equations are valid for natural porous polycrystalline rocks both in the drained (fluid or melt free) and undrained state. In the undrained state, the porous space is filled with an isotropic viscous substance, which can be a liquid, gas or fluid, characterized by a bulk modulus or inverse compressibility  $1/K_f = -\frac{1}{V} \frac{\partial V}{\partial P}$ . Specific poroelastic effects cause a strong dependence of seismic velocities on frequency for fluid or melt saturated rocks (Cheng, 2016), however, usually these effects occur in a frequency range higher than that used in geophysical practice.

In the theory of the poroelasticity, undrained bulk modulus is defined as a function of the drained modulus and Biot constant  $\alpha$ . The Biot constant  $\alpha$  is a fundamental parameter of a poroelastic material and is equal to the loss (or gain) of fluid volume as a fraction of the change in volume ( $\alpha < 1$ ) of the deformed material at constant fluid pressure. For a homogeneous isotropic rock, these relations for the undrained bulk modulus  $K_u$  and Poisson ratio  $\nu_u$  read as (Cheng, 2016):

$$K_u = K_s \left( 1 + \frac{\alpha^2 K_f}{(1 - \alpha)(\alpha - \phi) K_f + \phi K} \right), \quad (2)$$

$$v_u = \frac{3K_u - 2G}{2(3K_u + G)},$$

where  $K$  and  $G$  are the parameters of the porous matrix material,  $K_s$  is the bulk modulus of the mineral that the matrix consists of,  $\phi$  is the porosity and the general expression for the Biot's coefficient  $\alpha$ :

$$\alpha = 1 - \frac{K}{K_s}, \quad (3)$$

where  $K_s$  is the bulk modulus of the solid phase constituting the porous matrix. For isolated spherical pores, the Biot constant  $\alpha$  can be estimated (Simakin and Ghassemi, 2004):

$$\alpha = \frac{3\phi(1 - \nu)}{2(1 - 2\nu) + \phi(1 + \nu)}. \quad (4)$$

This estimate is only slightly higher than the theoretical lower limit of the Biot constant  $\alpha \geq 3\phi/(2 + \phi)$  (Cheng, 2016) and equals to it in the limit  $\nu = 0$ . The measurement data of real rocks showed that even at low porosity, the values of the Biot constant  $\alpha$  are usually up to 4–5 times higher than the lower limit, depending on the texture of the porous space (see Fig. 1). For a simplified geometry (oblate spheroid or ellipsoid with radii  $r_1 > r_2 = r_3$  and aspect ratio  $\theta = r_2/r_1$ ) of evenly distributed pores, drained mechanical parameters were calculated (Wu, 1966; Berryman, 1980; Schmeling, 1985). Takei (2002), based on the oblate spheroid model, expressed the drained moduli as a linear function of porosity  $\phi$ :

$$K = K_s(1 - k_1(\theta)\phi), \quad G = G_s(1 - k_2(\theta)\phi). \quad (5)$$

Biot constant was expressed by Eq. (2), based on the values of coefficient  $k_1$  for  $\nu = 0.25$  from (Takei, 2002). This allows us to calculate the value of  $V_p/V_s$  given the porosity ( $\phi$ ) and relative compressibility of the fluid ( $K_f/K_s$ ) plotted in Fig. 2. In calculations we vary porosity up to 4% and the ratio  $K_f/K_s$  from 1 (upper limit for magma) to 0.001 which is close to the value for the ratio of CO<sub>2</sub> fluid compressibility at  $T = 1100^\circ\text{C}$  and  $P = 1$  kbar,  $K_f \approx 0.1$  GPa (calculated with model Kerrick and Jacobs (1981)) and forsterite bulk modulus  $K_s \approx 100$  GPa (Bejina et al., 2021). In tectonically active areas, a spheroid with a small aspect ratio ( $\theta \ll 1$ ) can be interpreted as a crack, and a sphere ( $\theta = 1$ ) as an inclusion in a mineral.

The undrained bulk modulus  $K_u$  (and  $V_p$ ) is larger for connected pores (e.g. in the fractured rocks) than for rocks with isolated pores (fluid inclusions in minerals). Structural transition from inclusions to cracks due to poro-elastic effects provides variation of  $V_p/V_s$  ratio up to 10–14% (see Fig. 2). For transverse isotropic (layered) fluid saturated rocks, the effect of the

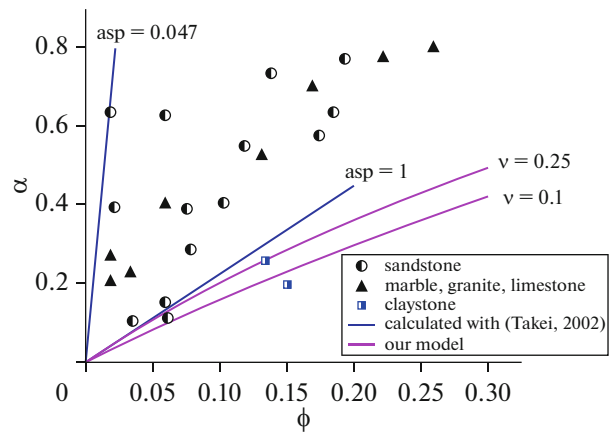


**Fig. 1.** Biot constant  $\alpha$  versus porosity, measurements data from (Cosenza et al., 2002), orange lines with values calculated from the oblate spheroid model (Takei, 2002) at  $\nu = 0.25$  and various geometric ratios of spheroid axes  $\gamma = r_a/r_b$ , pink lines calculated by equation (3) at  $\nu = 0.25$  and  $\nu = 0.1$ .

pores aspect ratio on seismic velocities is considered in (Hong-Bing et al., 2013).

According to the above analysis, an isotropic porous solid with fluid-filled pores has  $V_p/V_s$  lower and melt-filled higher than drained pore rock. Similarly, low  $V_p/V_s$  and high  $V_p/V_s$  anomalies in the geothermal areas are interpreted as porous rocks filled predominantly with steam and liquid water, respectively (Gunasekera et al., 2003).

In some cases, porous rocks may contain both fluid and melt. Partial rhyolitic melts with exsolved fluid in the Krafla volcano caldera at a depth of 3.5 km appear as a low  $V_p/V_s$  anomaly, which is explained by the prevailing effect of fluid on seismic velocities (Schuler et al., 2015; Simakin and Bindeman, 2022). We will interpret low  $V_p/V_s$  anomalies as a fluid reservoir by the dominant factor, which cannot rule out the presence of a melt there.

At the same time, high  $V_p/V_s$  values can be an indication of a specific phase composition, for example, serpentinized mafic rocks, which is used at the interpretation of seismic data for a subducted slab and mantle wedge (e.g., Carlson and Miller, 2003). In interpreting seismic data from the crust over the Kamchatka mantle wedge, we assume that  $V_p/V_s$  variations, especially rapid temporal changes, are due to poro-elastic effects in common rock types.

### Kamchatka

The theoretical fundamentals discussed above provide a solid basis for interpreting seismic data on the state of the fluid and partial melt in the mid-deep crust of subduction zone in Kamchatka. The highly active volcanoes of the Klyuchevskaya group (KGV) and the nearby Shiveluch volcano (Northern Kamchatka),

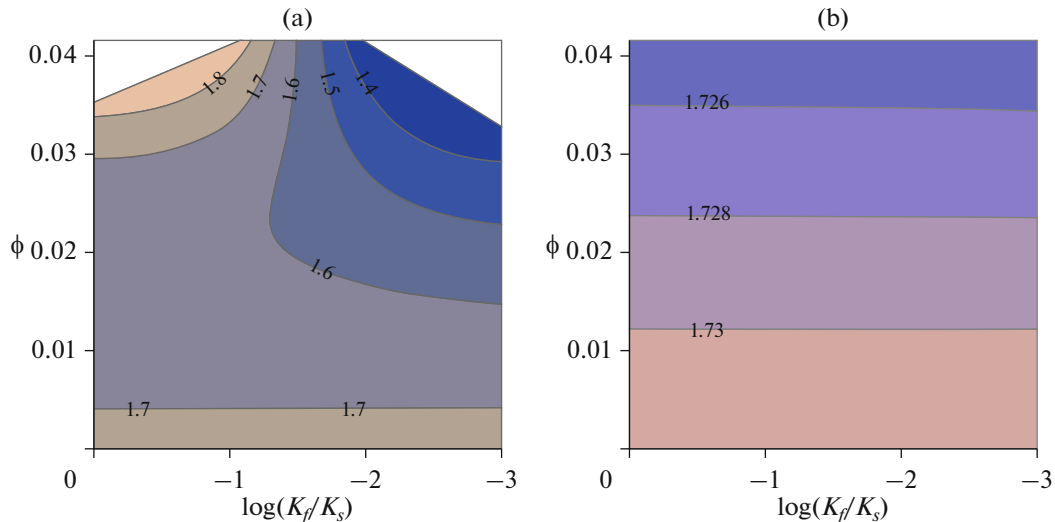


**Fig. 2.**  $V_p/V_s$  ratio calculated as a function of porosity ( $\phi$ ) and  $z = \log(K_f/K_s)$ , where  $K_f$  and  $K_s$  are bulk moduli of the fluid and the solid phase that makes up the porous matrix, respectively; the values of parameters used in the calculations (a) for fractures—shape factor  $\gamma = 0.04$ , coefficients in formulas (5)  $k_1 = 25.60$ ,  $k_2 = 9.96$  (b) inclusions— $\gamma = 0.63$   $k_1 = 2.32$ ,  $k_2 = 1.98$  (see text for explanation). It can be noted that nearly spherical inclusions have a much weaker effect on the  $V_p/V_s$  ratio than crack-like inclusions.

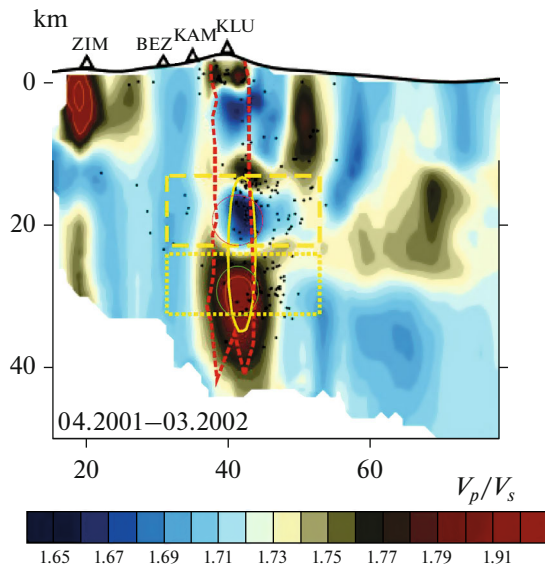


**Fig. 3.** Shown is the SSW-NNE section of a 3D tomographic image obtained by processing the earthquake signals of 04.2001–03.2002 after (Koulakov et al., 2013), paired  $V_p/V_s$  anomalies indicated by red (low values) and green (high values) ellipsoids under Klyuchevskoy volcano (ZIM—Zimina, BEZ—Bezymianny, KAM—Kamen, KLU—Klyuchevskoy volcanoes). The red short dashed line marks the magma cracking system under the Klyuchevskaya volcano according to (Kiriyukhin et al., 2020). The yellow rectangles outline the vertical position of two intervals of intense seismicity after (Koulakov et al., 2013). The yellow vertical ellipsoid is the isoline of the rocks electrical conductivity 20 Ohm m from the MTS survey (Moroz and Loginov, 2016), showing the depth, lateral and vertical dimensions of the zone of low resistance under the Tolbachik volcano after the 2012–2013 eruption (located outside the seismic profile, 30 km southwest of Klyuchevskoy volcano).

one of the most active on the Earth, as well as Avachinsky volcano (Southern Kamchatka), known for its abundance of peridotite xenoliths, have been most fully characterized by geophysical and petrological methods and will be considered below.

### KGV SEISMIC TOMOGRAPHY

Koulakov et al. (2013) published the results of seismic tomography in the KGV region, providing information on processes in the Earth's crust over the period 1999–2009. In the vertical sections of the  $V_p/V_s$  distribution with NNE-SSW orientation through the Klyuchevskoy volcano, one can distinguish a boundary at a depth of 14–17 km, corresponding to the brittle-ductile rheological transition (BDT) (Fig. 3). Systematic observations showed the appearance and disappearance of large volumes with anomalous  $V_p/V_s$  ratios with low values up to 1.65 (–2.9% of the mean 1.70) and high values up to 1.83 (+7.6%) (see Figs. 3, 4). These anomalies are located under Klyuchevskoy volcano at depths below the BDT with centers of 17 and 30 km, respectively. Previously, Koulakov (2012) associated high  $V_p/V_s$  anomalies with magma storage zones below the volcano. However, this interpretation contradicts the practical disappearance of anomalies and their appearance within months.

### SPATIAL RESOLUTION OF SEISMIC DATA

The accuracy and reliability of the tomography results in (Koulakov et al., 2013) was ensured by a synthetic test with the inclusion of model objects with

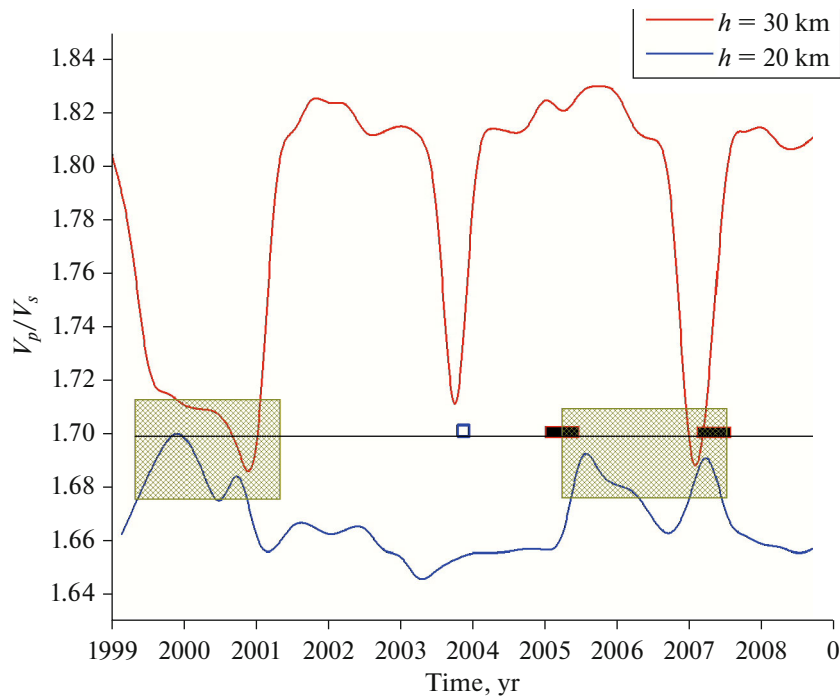


**Fig. 4.** Changes in the  $V_p/V_s$  ratio in paired deep anomalies under Klyuchevskoy volcano, estimated from the results of seismic tomography by Koulakov et al., (2013) (extreme values are used in the areas indicated in Fig. 3) depending on time. The unperturbed by poroelastic effects mean value of about 1.7 (baseline) is marked with a solid horizontal line. Several episodes when  $V_p/V_s$  in both anomalies approached the baseline are outlined with cross-hatched rectangles. Blue open box and red filled boxes on the baseline show episodes of magma upwelling and Strombolian eruptions of Klyuchevskoy Volcano (Koulakov et al., 2013), respectively.

anomalous  $V_p$  and  $V_s$  with sizes of about  $5 \times 5$  km. Later, Koulakov et al., (2017) published the results of seismic tomography in the KGV area based on observations in 2014–2015 using additional 22 stations of the temporary seismic network. Checkerboard test (cells  $7 \times 6$  km) showed good resolution down to a depth of 10 km and worse resolution below.

Comparison of active  $V_p/V_s$  anomalies under Klyuchevskoy volcano in 2004 (Koulakov et al., 2013) and according to data (Koulakov et al., 2017) showed that in the latter case, an anomaly of low  $V_p/V_s$  values centered at a depth of about 20 km stretched deeper and change the configuration. The deep high  $V_p/V_s$  anomaly (25–35 km) is closely reproduced, its horizontal size is about 10 km, which approximately corresponds to the diameter of magma fracking system under the Klyuchevskoy volcano, extended from the Moho (35 km) to the surface according to the data (Kiryukhin et al., 2020). A positive anomaly can be interpreted as a volume of rock with a melt content of a few vol %, and a negative anomaly as a reservoir of fluid with  $n \times 0.1$  vol % fluid. Detailed seismic information for the entire crust and upper mantle in the region of Avachinsky volcano, similar to that considered above for the KGV, is not available.

### *MTS Kamchatka*

In the large-scale magneto-telluric sounding (MTS) survey (Moroz and Gontovaya, 2017), under the KGV and Avacha-Koryaksky volcanoes, zones of increased electrical conductivity  $\rho = 5\text{--}10$  Ohm m were identified in the depth interval of 15–37 km. Moroz and Loginov (2016) presented the results of a detailed MTS profiling performed in 2014 in the area of the 2012–2013 Tolbachik volcano eruption, which is consistent with a large-scale study. The measurements along profiles 8–15 km long were interpreted down to a depth of 60 km. An area of high conductivity was found in a narrow zone of 3–4 km with a resistivity  $\rho < 10$  Ohm m under the source of fissure eruption at depths of 14–31 km, which extends to a depth of 35 km with  $\rho < 20$  Ohm m. When the MTS data under Tolbachik are superimposed on the vertical section of the  $V_p/V_s$  ratio under the Klyuchevskoy volcano (measured in 2001) from (Koulakov et al., 2013), the area bounded by the low resistance isoline ( $\rho < 10$  Ohm m) overlaps with the combined zones of low and high  $V_p/V_s$  anomalies. As follows from the above discussion, low  $V_p/V_s$  values correspond to a fluid reservoir and high  $V_p/V_s$  values correspond to a partial melt, both with low resistivity.

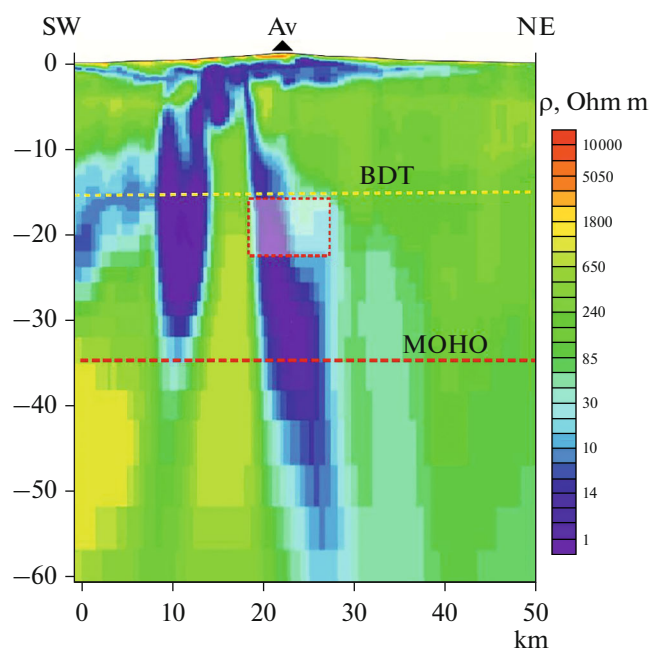


**Fig. 5.** Conductivity profile across the coastline of Kamchatka passing through Avachinsky volcano (Av), MTS survey (Moroz and Loginov, 2019). The Moho position is shown after (Levin et al., 2002), the position of the brittle-ductile rheological transition (BDT) is hypothetical, as in Northern Kamchatka, consistent with the horizontal boundary on the profile. The dotted translucent rectangle shows the depths of equilibration of xenolith minerals, estimated using geobarometers, and the content of volatiles in MIs (see text).

A detailed MTS survey under the Avacha-Koryaksky volcanoes revealed two continuous deep fluid-magma transport systems with low resistivity down to mantle depths of 35 and 55 km (Moroz and Loginov, 2019). Figure 5 shows resistivity sections with superimposed positions of Moho and brittle-ductile rheological transition boundary along with xenolith formation depth interval. This figure clearly shows a deep transverse fault extending into the upper mantle as a highly conductive fluid transport zone. Authors estimated that, an electrically connected pore space providing an observed minimum conductivity of 1–5 Ohm m is estimated to be as low as 0.1% by volume for fluid and about 1 vol % for melt. These estimates can be lower than the total volume of connected melt and fluid in the rocks, which is able to lead to the observed variations of the seismic velocities and the  $V_p/V_s$  ratio.

#### *Interpretation of Geophysical Data*

Temporary disappearance of deep anomalies in 1999–2001 under KGV was explained by the complete closure of the entire pore space (“no melt, no fluid” Fig. 8 in Koulakov et al., 2013) and active transport of magma and fluids in other time periods. It is not possible to estimate exact fluid volumes in low and high

$V_p/V_s$  zones due to uncertainties in the interpretation of geophysical data. However, it is difficult to assume the transfer of at least several km<sup>3</sup> of magma or fluid in a short time. Solidification of large volumes of magma in a short time is also impossible. These observations can be explained by assuming that the variations in seismic velocities are largely caused by thermal (hydro)- fracturing of fluid (melt) saturated rocks, increasing Biot constant  $\alpha$  and thus decreasing (increasing)  $V_p/V_s$ . At high  $P$ - $T$  below BDT, the fractures heal with the formation of fluid and melt inclusions on a time scale of several months.

Koulakov et al. (2013) presented data on cumulative seismicity under the KGV in terms of depth and time for the period 1999–2010. Two separate intervals of intensive seismicity are clearly distinguished at the depths of 14–28 km (average 21 km) and 24–32 m (average 28 km), which can be associated with the above mentioned zones of low and high  $V_p/V_s$ , respectively (see Fig. 3). Three episodes of high seismicity in the upper zone with time centers: January 2004, March 2005, and April 2007 occurred during magma upwelling and two eruptions of Klyuchevskoy volcano, respectively (see Fig. 4). During these periods, seismic activity in the lower zone decreased after rising in the time preceding magmatic activity. The periods of eruptions coincide with the disappearance of the anomaly with low  $V_p/V_s$  and partially high  $V_p/V_s$  (the second eruption). Quiet seismic period 1999–June 2001 corresponds to the disappearance of both anomalous zones in 1999–2001 (Fig. 4). The 2005 and early 2007 eruptions were of the Strombolian style. The Strombolian style at Stromboli and Etna has been shown to be caused by flushing of magma in the Earth’s crust with a CO<sub>2</sub>-enriched fluid, creating bubbly magma at depth (Caricchi et al., 2018). In the case of Klyuchevskoy Volcano, the temporary disappearance of low  $V_p/V_s$  anomalies during Strombolian eruptions can be interpreted as a manifestation of the transition of fluid from an activated crustal reservoir to magma with a decrease in overpressure and a morphological transition in the structure of the pore space of reservoir rocks, as discussed above.

#### LINK BETWEEN GEOPHYSICAL AND PETROLOGICAL DATA

The low and middle crustal fluid reservoirs of the active continental margin of Kamchatka, characterized indirectly from geophysical data, cannot be accessed by drilling. Information about the state of fluids and rocks in such reservoirs can be obtained from the study of xenoliths in volcanic rocks. Such xenoliths can be unconsolidated active cumulates (also called enclaves) containing an interstitial melt of the allvalite type (Plechov et al., 2008). Or they may be fragments of solidified ultramafic-mafic intrusions expected under active volcanoes, including the KGV

(Khubunaya et al., 2007). The next section will consider the reinterpretation of published petrological data from Kamchatka.

### *Xenoliths*

As it rises from its generation level, magma tends to accumulate at the boundaries of contrasts in density and mechanical properties (Gudmundsson, 2011). For example, as shown experimentally (Kavanagh et al., 2006), in a two-layer elastic system, the liquid stagnates under upper layer when its rigidity (elastic stiffness proportional to Young modulus) is higher than that of the lower one. The lower level of accumulation is the Moho boundary. At midcrustal depths, the rheological properties of rocks pass through a brittle-ductile transition (BDT). The depth of the BDT is temperature dependent and can be locally reduced by magma heating (from 15.7 to 7.5 km in the case analyzed by de Silva and Gosnold (2007).

The specific localization of the BDT depends on the composition of the rocks, the thermal gradient (Paterson and Wong, 2005; Brace and Kohlstedt, 1980), and the characteristic strain rates driven by the kinematics of the geodynamic conditions. For example, for a strain rate  $1.0e-5s^{-1}$ , quartz rheology, and a temperature gradient of  $18^{\circ}C/km$ , the BDT depth (interpreted as depth with differential stress less than 1 kbar) is estimated at 15 km (Brace and Kohlstedt, 1980).

### KGX XENOLITHS

The mafic xenoliths from the lavas of the active volcanoes of KGV and Shiveluch are predominantly magmatic cumulates, bearing information about the  $P$ - $T$  conditions of their formation. Mineralogical thermo-barometers are especially effective for minerals from magmatic cumulates, which have a long residence time at a high temperature of about  $1000^{\circ}C$  and are often mutually equilibrated.

Ionov et al., (2013) reported on the mineral composition of ultramafic xenoliths of Bezymyanni Volcano (KGV). The amphibole composition indicated a pressure of 4.2 kbar using the latest version of the amphibole barometer from (Simakin et al., 2019). A two-pyroxene geothermobarometer (Putirka, 2008) (values calculated by formulas (38) and (39) the latter is enclosed in brackets) for the same xenoliths gives  $P = 6.1 \pm 1.6$  kbar ( $4.8 \pm 1.9$ ),  $T = 927 \pm 10^{\circ}C$  ( $n = 2$ ). A close pressure value of  $5.9 \pm 0.5$  ( $4.4 \pm 0.3$ ) kbar at  $T = 927 \pm 10^{\circ}C$  ( $n = 4$ ) follows from the analyses of  $Opx$ - $Cpx$  pairs from the mafic xenoliths of the Bezymyanni volcano given in (Davydova et al., 2018). Two-pyroxene geothermobarometry is less reliable for the composition of phenocrysts in lava, since crystals can reflect different stages of magma evolution at different  $P$ - $T$  parameters. Ozerov (2000) reported compositions of a number of host clinopyroxenes ( $n = 4$ )

and their orthopyroxene inclusions ( $n = 3$ ) from the high-aluminum basalt of Klyuchevskoy Volcano, which promised better results than the use of separate phenocrysts. Since no information was provided on the relative position of the analyzed grains, all possible pairs were considered. Out of the 12 pairs two meet the equilibrium criteria according to (Putirka, 2008) and give an average of 4.5 (5.1) kbar close to the above estimates. The mean value obtained with two-pyroxene barometer for xenoliths lithostatic pressure of 5.4 kbar corresponds to a depth of 20 km with an average rock density of  $2750 kg/m^3$ . The distribution of rock density for the KGV from (Fedotov et al., 2010) gave almost the same depth of 20.3 km. The pressure range of 4–6 kbar for xenolith equilibration closely matches seismic data for a low  $V_p/V_s$  fluid reservoir (Fig. 3).

### AVACHINSKY VOLCANO XENOLITHS

The peridotite xenoliths of Avachinsky volcano are known for the finds of the native Ni and Fe (Ishimaru et al., 2009) and olivines with an unusually high content of NiO of up to 5.3 wt % (Ishimaru and Arai, 2008b). These xenoliths have been studied in detail and described in a series of publications by Ionov (2010), Bénard et al. (2016), Ishimaru et al. (2007) and Ishimaru and Arai (2008a). The analyses of coexisting  $Opx$  and  $Cpx$  given in these publications indicate consistent pressure values of about 5 kbar (values according to formulas (38) and (39) in Putirka (2008)): Ionov (2010)  $5.2 \pm 1.2$  kbar ( $5.7 \pm 1.8$ ) ( $n = 3$ ); Bénard et al., (2016)  $5.2 \pm 1.2$  kbar ( $5.7 \pm 1.8$ ) ( $n = 2$ ); Ishimaru et al., (2007)  $4.4 \pm 0.7$  kbar ( $4.9 \pm 0.7$ ) ( $n = 3$ ). Our amphibole barometer (Simakin et al., 2019) based on compositions from Ishimaru et al. (2007) and Ishimaru and Arai (2008a) gave 4.5 kbar. The compositions of pyroxenes from the same sample were used for barometry, but this does not guarantee their equilibration. In this regard, the most reliable values have been obtained for the compositions of daughter  $Opx$  and  $Cpx$  in melt inclusions in spinel by Bénard et al., (2016). Two values of pressure calculated with equations 38 and 39 from Putirka (2008) are plotted in Fig. 6 as a function of  $Al_2O_3$  content, which is proportional to undercooling at crystals growth. It can be noted that the two values practically coincide at a low  $Al_2O_3 < 2.3$  wt % and give  $5.2 \pm 1.7$  kbar ( $4.9 \pm 0.7$ ) ( $n = 3$ ). In the MTS section (Fig. 5), the zone of xenolith formation under Avachinsky volcano is not expressed against the background of the predominant electrically conductive zone of deep mantle fluid transfer.

In all the publications discussed above, the ultramafic Avacha xenoliths were interpreted as upper mantle xenoliths, which contradicts the results of mineralogical barometry and, as will be discussed below, the content of volatiles in melt inclusions.

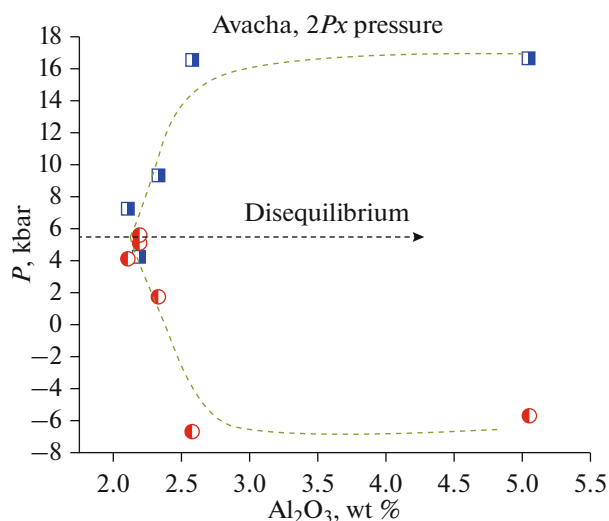


**Fig. 6.** Equilibrium pressure estimates for *Cpx*-*Opx* pairs from melt inclusions in spinel from mafic xenoliths of Avacha Volcano depending on the  $\text{Al}_2\text{O}_3$  content in *Cpx* (data from supplementary file to (Bénard et al., 2016)). The estimates by the two formulas from Putirka (2008) (squares—eqn.(), circles—eqn.()) merge for pairs with a low content of  $\text{Al}_2\text{O}_3$  in *Cpx* approaching equilibrium.

#### Volatiles in Melt Inclusions

Melt inclusions (MIs) in olivine provide a record of information about processes proceeding at magma accumulation levels. Water quickly leaves the MIs in olivine (Portnyagin et al., 2019), therefore, reliable data can only be obtained by studying olivines from naturally quenched scoria or crystals blown out of magma. The highest contents of  $\text{CO}_2$  and  $\text{H}_2\text{O}$  in MIs in olivine from Tolbachik were reported by Gurenko (2021) and Zelenski et al. (2021). These data are plotted in Fig. 7 together with two experimental solubility isobars in basaltic melt at  $P = 4$  and 5 kbar from (Shishkina et al., 2010). On these isobars at low water content, the concentration of  $\text{CO}_2$  is almost constant, close to the experimental data on the solubility of  $\text{CO}_2$  at  $T = 1200^\circ\text{C}$  in the tholeiitic melt from (Pan et al., 1991), shown along the y-axis for pressures of 5, 6, 7 and 10 kbar. In Fig. 7, the volatiles contents of both Gurenko (2021) and Zelenski et al. (2021) corresponds to the maximum saturation pressures in the range 4–6 kbar, only few points are located around 7 kbar. Four points from MIs of the 1941 Tolbachik eruption (Zelenski et al., 2021) recorded a significantly higher saturation pressure of up to 10 kbar.

The content of volatiles in the melt in equilibrium with Avachinsky volcano mafic xenoliths was characterized by the analysis of MIs in spinel (Bénard et al., 2016). Spinel is a better host for MIs than olivine, protecting them from the fast water loss. The melt compositions are plotted in Fig. 7 together with Tolbachik data, the maximum saturation pressure is 6 kbar.

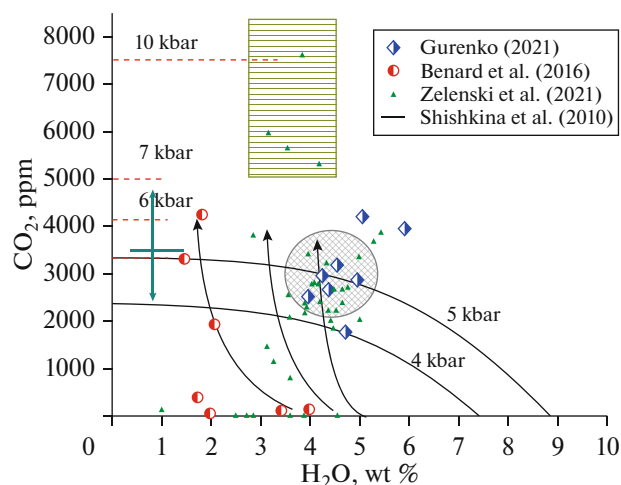


**Fig. 7.** Compositions of melt inclusions (MIs): red circles—MIs in spinel from the main xenoliths of Avacha volcano (data from supplementary file to (Bénard et al., 2016)), semi-filled diamonds—MIs in olivine from scoria of the Tolbachinsky eruption (Gurenko, 2021), green triangles—MIs in olivine from the 1941 Tolbachik volcano eruption (Zelenski et al., 2021). The compositions with the highest saturation pressure with equivalent depth approaching Moho are boxed. Solubility isobars in basaltic melt at  $T = 1250^\circ\text{C}$  and  $P = 4$  and 5 kbar according to (Shishkina et al., 2010) are shown by solid lines, dashed lines show  $\text{CO}_2$  solubility in dry tholeiitic melt at  $1200^\circ\text{C}$  (Pan et al., 1991). The arrows show the possible trajectories due to the fluxing of the hydrous melt (points on the abscissa axis with 3–4.5 wt %  $\text{H}_2\text{O}$ ) by the fluid enriched in  $\text{CO}_2$ .

It is important to note that there are data points with  $\text{CO}_2$  contents below the detection limit. Their water content is low up to 4–5 wt % and melts are unsaturated at  $P = 5$ –6 kbar. On the whole, the obtained data do not contradict the process of fluxing of magma with  $\text{CO}_2$ -enriched fluid in the crust. Due to the lower diffusivity of  $\text{CO}_2$ , water is first transferred into the fluid bubbles, and then the melt is enriched in  $\text{CO}_2$ , thus creating the compositions indicated by the arrows in Fig. 7. The trajectory of MIs from Avachinsky volcano is directed towards more water-deficient compositions, which may reflect a higher  $\text{CO}_2$  content in the fluid and a higher liquid/melt ratio.

Gurenko (2021) provided information on  $\delta^{34}\text{S}$  and  $\delta^{11}\text{B}$  isotope data, which may reflect fractionation at possible stages of dissolution and exsolution of fluid from the melt. However, probably due to complex interactions, they do not allow for simple interpretation. The four points with the highest saturation pressure according to Zelenski et al. (2021) can be interpreted as the compositions of the melts formed during flushing of magma with  $\text{CO}_2$  at a near Moho depth. Figure 8 shows that the sulfur content decreases with increasing  $\text{CO}_2$ , which is expected in the interaction of a  $\text{CO}_2$ -rich fluid dissolving in the melt with sulfur extraction by the fluid. The dense sulfur (higher  $^{34}\text{S}$

content) is fractionated into the fluid phase, thereby lightening the sulfur dissolved in the melt. Khubunaya et al., (2007) reported the observation of dense  $\text{CO}_2$  fluid inclusions in olivine from high-Mg basalts of Klyuchevskoy volcano with a capture pressure of 5–6 kbar. These inclusions can be formed when a  $\text{CO}_2$ -enriched fluid flushes magma that crosses the fluid reservoir at a midcrustal depth under the KGV.

The main part of presented data on the composition of the MIs indicate maximum saturation pressures in the range of 4–6 kbar, which is close to the estimates obtained using mineral barometers for mafic xenoliths. These pressure values correspond to depths of 15–22.5 km, if we take the density profile with depth from (Fedotov et al., 2010). This depth interval is in good agreement with the location of the low  $V_p/V_s$  zone in Fig. 4, which we interpret as a fluid reservoir in ultrabasic crustal cumulates. Only smaller part of MIs data with saturation pressure above 6–7 kbar can correspond to a seismic “deep magma chamber” or zone with high melt fraction and high  $V_p/V_s$  extending to the Moho depth (35–37 km according to (Levin et al., 2002) in Fig. 4. The high abundance of xenocrysts of chromium-bearing diopside and titanium garnets in multiphase inclusion in olivine from the 1941 Tolbachik eruption (Simakin et al., 2015) indicates their deep origin and direct transfer of magma from the near Moho depths to the surface, which is confirmed by the extremely high content of  $\text{CO}_2$  in some melt inclusions from the olivine (Zelensky et al., 2021). However, all mentioned above ultramafic xenoliths of the KGV and Avachinsky volcano classified as being of mantle origin (e.g., Ionov et al., 2013) are crustal cumulates. Khubunaya et al. (2007) argued for the picrite composition of the initial magma of Klyuchevskoy volcano. Ultrabasic-basic cumulates presented in xenoliths are a natural product of early *Ol* and *Ol-Opx* fractional crystallization of picritic magma. Whereas allivalite enclaves were formed during early *Ol-Pl* fractional crystallization of basaltic magma (Plechov et al., 2008).

The equilibration pressures of the considered xenoliths in the zone of low  $V_p/V_s$  values, interpreted as a reservoir of deep crustal fluid, is not accidental. Xenoliths are formed in the acts of mechanical failure of the reservoir due to hydraulic fracturing caused by the transfer of magma during an eruption and manifested by seismic activity. During the same process, fluidization of the magma occurs, which provides the Strombolian type of eruption.

## DISCUSSION

The key point of our model is the identification of ultramafic xenoliths in the lavas of North Kamchatka and Avachinsky volcanoes as cumulates located mainly in the zone of low  $V_p/V_s$  values. In both cases, there is a developed system of magma chambers along

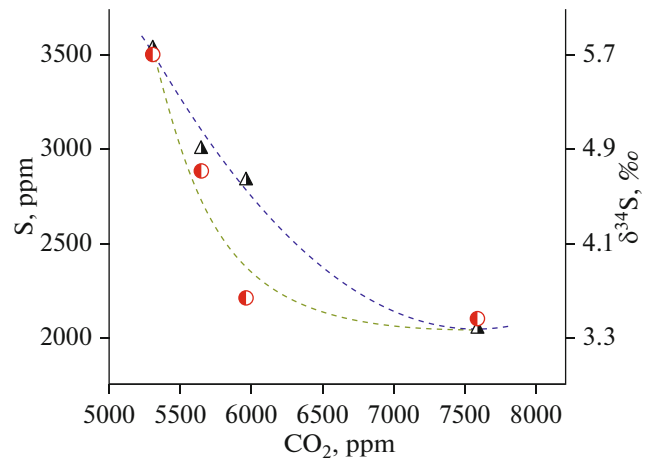


**Fig. 8.** The composition of MIs in olivine of the 1941 Tolbachik eruption (Zelensky et al., 2021), only points with high saturation pressure were selected (see Fig. 7). Total sulfur (triangles) and  $d^{34}\text{S}$  (circles) decrease with increasing  $\text{CO}_2$  content in the melt, as would be expected if sulfur passes into fluid bubbles together with  $\text{H}_2\text{O}$  during the fluxing of a magma with a  $\text{CO}_2$ -enriched fluid near the Moho depth.

the path of magma movement from the generation level to the surface. True mantle xenoliths can be expected for volcanoes with an undeveloped plumbing system, for example, at the initial stage of the formation of a Hawaiian type shield volcano (Canary Islands, Hawaii) or in monogenic cones and kimberlite pipes.

For example, lherzolite to pyroxenite ultramafic xenoliths in basanite cinder cones of the Deadman Lake Volcanic Field, California have been extensively studied for decades (Wilshire et al., 1980). In particular, several Dish Hill xenoliths from this volcanic field have a maximum pressure of 1–1.1 GPa as measured by a two-pyroxene barometer using mineral compositions from (McGuire et al., 1991). A somewhat lower maximum pressure value of 9.5 kbar was obtained using our amphibole geobarometer from amphibole compositions of abundant kersutite veins (Simakin and Shaposhnikova, 2017). Both estimates correspond to the mantle lithosphere sampled at a depth near the Moho by low-volume intraplate volcanism.

Probably, the contact of mantle magmas and the lower crust in the Pannonian alkaline-basalt province (Neogene age) is one of the best characterized places by various petrological methods. It demonstrates good agreement with all pressure estimates and thus the applicability of two-pyroxene geo-barometry of the Putirka (2008). The published pyroxenes compositions of ultrabasic xenoliths from alkaline basalts (Créon et al., 2017) yielding  $P = 1.1\text{--}1.3$  GPa,  $T = 1100^\circ\text{C}$  confirm their mantle origin. The composition of Kersutite amphibole (Torok et al., 2005) from low-crustal granulite (amphiboles are in association with

the melt) gives a pressure of 0.9 GPa. The maximum density of CO<sub>2</sub> fluid inclusions in clinopyroxene of mantle xenoliths is 1.0–1.1 g/cm<sup>3</sup>, which corresponds to a pressure of about 1.0 GPa at  $T = 1100\text{--}1150^\circ\text{C}$ . Maximum concentration of CO<sub>2</sub> in MIs is 9600 ppm corresponding to a saturation pressure of 1.2–1.3 GPa based on the calibration of Pan et al., (1991) in agree with the  $2Px$  barometer estimate. Equivalent depths of formation of mantle xenoliths at an average density of 2700 kg/m<sup>3</sup> are 41.5–49 km and for granulite—34 km. Basalts intruded and carried xenoliths at the stage of rift initiation in the thick crust (with the modern Moho depth of about 25–28 km).

#### *Comparison with Other Subduction Zones*

The presence of a fluid reservoir in the deep crust in North Kamchatka may be common to other subduction zones. For example, a similar interpretation of seismic data was proposed in (Nakajima et al., 2001) for Northeast Japan. Mid-crustal (depth 10–15 km) zones with low  $V_p/V_s$  are classified by the authors as reservoirs with aqueous fluid directly above the zone of partial melting (high  $V_p/V_s$ ). Sub-horizontal  $S$ -wave reflectors are localized mainly at the base and within the proposed fluid reservoir. The shallower location of the fluid reservoir likely reflects the higher measured heat flow in Northeast Japan than in North Kamchatka (Davies, 2013).

There are direct observations of how the fluid released in subducting plate rises in the mantle wedge and the overriding plate. An MT study in New Zealand (Wannamaker et al., 2009) demonstrated that the fluid released during the dehydration of the subducting slab accumulates in discrete portions in the crust below the brittle–ductile transition (BDT) boundary (depth 12–20 km), corresponding to the sequential decomposition of various hydrous phases. At a depth of about 12 km below BDT level, sub-horizontal fractures filled with fluid are assumed. Above these zones of fluid accumulation, thrusts are localized in the brittle upper crust. The Moho boundary in this area is at the depths of 25–30 km.

The migration of fluids in the Earth's crust can be affected by intense deformations and stresses caused by glaciation-deglaciation cycle. The effect of post-glacial activation of volcanic activity in the early Holocene was quite noticeable in Northern Kamchatka. It was marked by extremely explosive eruptions of a large volume of Pleistocene volcanoes in the Central Kamchatka Depression. The first eruptions of new volcanic centers that arose in the Holocene (Klyuchevskoy volcano, Tolbachik, Molodoy Shiveluch) were also highly explosive (for example, (Ponomareva et al., 2013)). The high explosiveness of the Early Holocene eruptions can be explained by the influence of fluid reservoirs in the lower crust formed during postglacial deformations. Deglaciation affects volcanism by

accelerating the rate of magma generation if the adiabatic decompression mechanism is involved (Pagli and Sigmundsson, 2008; Maclennan et al., 2002). Simakin and Murav'ev (2017) showed using numerical simulations that glaciation/deglaciation also induces deviatoric stress, which increases several times above the low-viscosity magma accumulation zone assumed in the model at a depth of 35 km. The level of deviatoric stresses is sufficient for hydraulic fracturing, which can create deep reservoirs for fluid accumulation. Magma following a new path initiated by the post-glacial stress state will be subjected to fluid flushing at depth when crossing such a reservoir, which increases the rate of magma uplift and the explosiveness of the eruption.

In conclusion, we note that all the signs of mantle metasomatism observed in the mafic xenoliths of the Avachinsky (Ishimaru et al., 2007) and Klyuchevskoy (Ionov et al., 2013) volcanoes, taking into account the improved depth of localization of xenoliths in the crust presented above, become a source of information on fluid transport and fluid-rock interaction in ductile magmatic cumulates at high PT. These data may improve our understanding of the mechanism of rapid fluid migration in the ductile lower crust of tectonically active zones, expected from surface observations (e.g., Kennedy and van Soest, 2007). Undoubtedly, this mechanism differs from that predicted for a stable continental crust by the porosity wave theory (Connolly and Podladchikov, 2013). Periodic rock failure on a time scale much smaller than the compaction scale implied by the geophysical data discussed above will result in pressure homogenization and pore space reconnection, invalidating the simplified porosity wave solution.

## CONCLUSIONS

- 1) The transition from the state of hydraulically connected fractures to isolated pores (healed cracks) filled with fluid or melt may be the reason for the temporary disappearance of low and high  $V_p/V_s$  anomalies, respectively on a scale of several months, observed under Klyuchevskoy volcano.
- 2) The anomalous zone of low  $V_p/V_s$  at depths centered at 20 km, which is also characterized by high electrical conductivity under the KGV, can be a low-crustal fluid reservoir.
- 3) The mafic xenoliths of the KGV and Avacha volcanoes are magmatic cumulates formed at pressure  $5.5 \pm 1.5$  kbar, the value of which is consistently estimated from mineral barometers and data from melt inclusions.
- 4) Xenoliths were extracted from a fluid reservoir hosted in magmatic cumulates when magma rising from the underlying storage level crossed it.

## ACKNOWLEDGMENTS

The authors thank Yury Taran for useful criticism of the early version of this work and Alexey Ariskin for a comprehensive review of the final version of MS. Vera Devyatova made an invaluable contribution to the analysis of the mafic xenoliths and inclusions of the Shiveluch volcano, which aroused interest in the crustal cumulates of Kamchatka. AGS is grateful to Maria Tolstykh and Andrey Babansky for the opportunity to visit the volcanoes of Northern Kamchatka during the 2007 field works.

## CONFLICT OF INTEREST

The authors declare that they have no conflicts of interest.

## REFERENCES

- Ba, J., Xu, W., Fu, L.Y., Carcione, J.M., and Zhang, L., Rock anelasticity due to patchy saturation and fabric heterogeneity: a double porosity model of wave propagation, *J. Geophys. Res.: Solid Earth*, 2017, vol. 122, no. 3, pp. 1949–1976.  
<https://doi.org/10.1002/2016JB013882>
- Bejina, F., Bystricky, M., Terce, N., Whitaker, M., and Chen, H., Equation of state and sound wave velocities of fayalite at high pressures and temperatures: implications for the seismic properties of the martian mantle, *Eur. J. Mineral.*, 2021, vol. 33, no. 4, pp. 519–535.
- Bekaert, D.V., Turner, S.J., Broadley, M.W., Barnes, J.D., Halldorsson, S.A., Labidi, J., Wade, J., Walowski, K.J., and Barry, P.H., Subduction-driven volatile recycling: a global mass balance, *Annu. Rev. Earth Planet. Sci.*, 2021, vol. 49, pp. 37–70.
- Bénard, A., Nebel, O., Ionov, D.A., Arculus, R.J., Shimizu, N., and Métrich, N., Primary silica-rich picrite and high-Ca boninite melt inclusions in pyroxenite veins from the Kamchatka sub-arc mantle, *J. Petrol.*, 2016, vol. 57, no. 10, pp. 1955–1982.
- Berryman, J.G., Long-wavelength propagation in composite elastic media II. Ellipsoidal inclusions, *J. Acoust. Soc. Am.*, 1980, vol. 68, no. 6, pp. 1820–1831.
- Berryman, J.G., *Mixture theories for rock properties, Rock Physics and Phase Relations: A Handbook of Physical Constants*, Ahrens, T.J., Ed., Washington, American Geophysical Union, 1995, vol. 3, pp. 205–228.
- Brace, W.F. and Kohlstedt, D.L., Limits on lithospheric stress imposed by laboratory experiments, *J. Geophys. Res.* *Solid Earth*, 1980, vol. 85, no. B11, pp. 6248–6252.
- Breeding, C.M. and Ague, J.J., Slab-derived fluids and quartz-vein formation in an accretionary prism, Otago Schist, New Zealand, *Geology*, 2002, vol. 30, no. 6, pp. 499–502.
- Burton, M.R. and Sawyer, G.M., Deep Carbon Emissions from Volcanoes, *Rev. Mineral. Geochem.*, 2013, vol. 75, pp. 323–354.
- Caricchi, L., Sheldrake, T.E., and Blundy, J., Modulation of magmatic processes by CO<sub>2</sub> flushing, *Earth Planet. Sci. Lett.*, 2018, vol. 491, pp. 160–171.
- Carlson, R.L. and Miller, D.J., Mantle wedge water contents estimated from seismic velocities in partially serpentinized peridotites, *Geophys. Res. Lett.*, 2003, vol. 30, no. 5, pp. 1250.  
<https://doi.org/10.1029/2002GL016660>
- Cheng, A.H.D., *Poroelasticity. Theory and Applications of Transport in Porous Media*, Springer Int. Publ., 2016, vol. 27.  
<https://doi.org/10.1007/978-3-319-25202-5>
- Connolly, J.A.D. and Podladchikov, Y.Y., A hydromechanical model for lower crustal fluid flow, *Metasomatism and the Chemical Transformation of Rock. Lecture Notes in Earth System Sciences*, Berlin–Heidelberg: Springer, 2013, pp. 599–656.  
[https://doi.org/10.1007/978-3-642-28394-9\\_14](https://doi.org/10.1007/978-3-642-28394-9_14)
- Cosenza, P., Ghoreychi, M., de Marsily, G., Vasseur, G., and Violette, S., Theoretical prediction of poroelastic properties of argillaceous rocks from in situ specific storage coefficient, *Water Resour. Res.*, 2002, vol. 38, no. 10, pp. 251–2512.  
<https://doi.org/10.1029/2001WR001201>
- Créon, L., Rouchon, V., Youssef, S., Rosenberg, E., Delpéch, G., Szabo, C., Remusat, L., Mostefaoui, S., Asimow, P.D., Antoshechkina, P.M., Ghiorso, M.S., Boller, E., and Guyot, F., Highly CO<sub>2</sub>-supersaturated melts in the Pannonian lithospheric mantle—A transient carbon reservoir?, *Lithos*, 2016, vol. 286, pp. 519–533.  
<https://doi.org/10.1016/j.lithos.2016.12.009>
- Créon, L., Delpéch, G., Rouchon, V., and Guyot, F., Slab-derived metasomatism in the Carpathian–Pannonian mantle revealed by investigations of mantle xenoliths from the Bakony–Balaton Highland Volcanic Field, *Lithos*, 2017, vol. 286, pp. 534–552.
- Davies, J.H., Global map of solid Earth surface heat flow, *Geochem., Geophys., Geosyst.*, 2013, vol. 14, no. 10, pp. 4608–4622.  
<https://doi.org/10.1002/ggge.20271>
- Davydova, V.O., Plechov, P.Yu., Shcherbakov, V.D., and Perepelov, A.B., High-K basaltic trachyandesite xenoliths in pyroclastic deposits from the Bezymianny volcano (Kamchatka), *Russ. Geol. Geophys.*, 2018, vol. 59, no. 9, pp. 1087–1099.
- Fedotov, S.A., Zharinov, N.A., and Gontovaya, L.I., The magmatic system of the Klyuchevskaya group of volcanoes inferred from data on its eruptions, earthquakes, deformation, and deep structure, *J. Volcanol. Seismol.*, 2010, vol. 4, pp. 1–33.
- Gudmundsson, A., Deflection of dykes into sills at discontinuities and magma-chamber formation, *Tectonophysics*, 2011, vol. 500, nos. 1–4, pp. 50–64.
- Gunasekera, R.C., Foulger, G.R., and Julian, B.R., Reservoir depletion at the Geysers geothermal area, California, shown by four-dimensional seismic tomography, *J. Geophys. Res.: Solid Earth*, 2003, vol. 108, no. B3.  
<https://doi.org/10.1029/2001JB000638>
- Guo, Z., Qin, X., Zhang, Y., Niu, C., Wang, D., and Ling, Y., Numerical investigation of the effect of heterogeneous pore structures on elastic properties of tight gas sandstones, *Front. Earth Sci.*, 2021, vol. 9, p. 641637.  
<https://doi.org/10.3389/feart.2021.641637>
- Gurenko, A.A., Origin of sulphur in relation to silicate-sulphide immiscibility in Tolbachik primitive arc magma (Kamchatka, Russia): Insights from sulphur and boron isotopes, *Chem. Geol.*, 2021, vol. 576, pp. 120244.

- Hirth, G. and Kohlstedt, D., Rheology of the upper mantle and the mantle wedge: a view from the experimentalists, *Inside the Subduction Factory*, Eiler, J., Eds., 2013. <https://doi.org/10.1029/138GM06>.
- Hong-Bing, L.I., Jia-Jia, Z., and Feng-Chang, Y.A.O., Inversion of effective pore aspect ratios for porous rocks and its applications, *Chin. J. Geophys.*, 2013, vol. 56, no. 1, pp. 43–51.
- Horváth, F., Musitz, B., Balázs, A., Véghe, A., Uhrin, A., Nádor, A., Koroknai, B., Pap, N., Tóth, T., and Wórum, G., Evolution of the Pannonian basin and its geothermal resources, *Geothermics*, 2015, vol. 53, pp. 328–352.
- Ionov, D.A., Petrology of mantle wedge lithosphere: new data on supra-subduction zone peridotite xenoliths from the andesitic Avacha volcano, Kamchatka, *J. Petrol.*, 2010, vol. 51, nos. 1–2, pp. 327–361. <https://doi.org/10.1093/petrology/egp090>
- Ionov, D.A., Bénard, A., Plechov, P.Yu., and Shcherbakov, V.D., Along-arc variations in lithospheric mantle compositions in Kamchatka, Russia: first trace element data on mantle xenoliths from the Klyuchevskoy Group volcanoes, *J. Volcanol. Geotherm. Res.*, 2013, vol. 263, pp. 122–131. <https://doi.org/10.1016/j.jvolgeores.2012.12.022>
- Ishimaru, S., Arai, S., Ishida, Y., Shirasaka, M., and Okrugin, V.M., Melting and multi-stage metasomatism in the mantle wedge beneath a frontal arc inferred from highly depleted peridotite xenoliths from the Avacha volcano, southern Kamchatka, *J. Petrol.*, 2007, vol. 48, no. 2, pp. 395–433.
- Ishimaru, S. and Arai, S., Calcic amphiboles in peridotite xenoliths from Avacha volcano, Kamchatka, and their implications for metasomatic conditions in the mantle wedge, *Geological Society, London, Special Publications*, 2008a, vol. 293, no. 1, pp. 35–55. <https://doi.org/10.1144/SP293.3>
- Ishimaru, S. and Arai, S., Nickel enrichment in mantle olivine beneath a volcanic front, *Contrib. Mineral. Petrol.*, 2008b, vol. 156, pp. 119–131. <https://doi.org/10.1007/s00410-007-0277-6>
- Ishimaru, S., Arai, S., and Shukuno, H., Metal-saturated peridotite in the mantle wedge inferred from metal-bearing peridotite xenoliths from Avacha volcano, Kamchatka, *Earth Planet. Sci. Lett.*, 2009, vol. 284, nos. 3–4, pp. 352–360.
- Kavanagh, J.L., Menand, T., and Sparks, R.S.J., An experimental investigation of sill formation and propagation in layered elastic media, *Earth and Planetary Science Letters*, 2006, vol. 245, nos. 3–4, pp. 799–813.
- Kennedy, B.M. and van Soest, M.C., Flow of mantle fluids through the ductile lower crust: helium isotope trends, *Science*, 2007, vol. 318, no. 5855, pp. 1433–1436.
- Kerrick, D.M. and Jacobs, G.K., A modified Redlich-Kwong equation of state for H<sub>2</sub>O, CO<sub>2</sub>, and H<sub>2</sub>O–CO<sub>2</sub> mixtures at elevated pressures and temperatures, *American Journal of Science*, 1981, vol. 281, pp. 735–767.
- Khubunaya, S.A., Gontovaya, L.I., Sobolev, A.V., and Nizkous, I.V., Magma Chambers beneath the Klyuchevskoy Volcanic Group (Kamchatka), *J. Volcanol. Seismol.*, 2007, vol. 1, no. 2, pp. 98–118.
- Kiryukhin, A., Chernykh, E., Polyakov, A., and Solomatina, A., Magma fracking beneath active volcanoes based on seismic data and hydrothermal activity observations, *Geosci.*, 2020, vol. 10, no. 2, pp. 52. <https://doi.org/10.3390/geosciences10020052>
- Koulakov, I., Multiscale seismic tomography imaging of volcanic complexes, *Updates in Volcanology: A Comprehensive Approach to Volcanological Problems*, 2012, vol. 1, pp. 207–242. <https://doi.org/10.5772/24653>
- Koulakov, I., Gordeev, E.I., Dobretsov, N.L., Vernikovskiy, V.A., Senyukov, S., Jakovlev, A., and Jaxybulatov, K., Rapid changes in magma storage beneath the Klyuchevskoy group of volcanoes inferred from time-dependent seismic tomography, *J. Volcanol. Geotherm. Res.*, 2013, vol. 263, pp. 75–91.
- Koulakov, I., Abkadyrov, I., Al Arifi, N., Deev, E., Droznina, S., and Gordeev, E.I., West, M., Three different types of plumbing system beneath the neighboring active volcanoes of Tolbachik, Bezymianny, and Klyuchevskoy in Kamchatka, *J. Geophys. Res: Solid Earth*, 2017, vol. 122, no. 5, pp. 3852–3874. <https://doi.org/10.1002/2017JB014082>
- Levin, V., Park, J., Brandon, M., Lees, J., Peyton, V., Gordeev, E., and Ozerov, A., Crust and upper mantle of Kamchatka from teleseismic receiver functions, *Tectonophysics*, 2002, vol. 358, nos. 1–4, pp. 233–265.
- Li, J., Ding, X., and Liu, J., The role of fluids in melting the continental crust and generating granitoids: an overview, *Geosci.*, 2022, vol. 12, no. 8, pp. 285. <https://doi.org/10.3390/geosciences12080285>
- Maclennan, J., Jull, M., McKenzie, D., Slater, L., and Gronvold, K., The link between volcanism and deglaciation in Iceland, *Geochem., Geophys., Geosyst.*, 2002, vol. 3, no. 11, pp. 1–25. <https://doi.org/10.1029/2001GC000282>
- Markl, G. and Bucher, K., Composition of fluids in the lower crust inferred from metamorphic salt in lower crustal rocks, *Nature*, 1998, vol. 391, no. 6669, pp. 781–783.
- McGuire, A.V., Dyar, M.D., and Nielson, J.E., Metasomatic oxidation of upper mantle peridotite, *Contrib. Mineral. Petrol.*, 1991, vol. 109, pp. 252–264.
- Moroz, Y.F. and Gontovaya, L.I., Deep structure of Kamchatka according to the results of MT sounding and seismic tomography, *Russ. J. Pac. Geol.*, 2017, vol. 11, pp. 354–367.
- Moroz, Y.F. and Loginov, V.A., A geoelectric model for the area of the Tolbachik eruption (named after the 50 year anniversary of the Institute of Volcanology and Seismology), *J. Volcanol. Seismol.*, 2016, vol. 10, pp. 292–304. <https://doi.org/10.1134/S0742046316050055>
- Moroz, Y.F. and Loginov, V.A., Deep geoelectrical model of the Avacha–Koryaksky group of volcanoes, Kamchatka, *Vestn. KRAUNTS. Nauki o Zemle*, 2019, vol. 2, no. 42, pp. 9–24.
- Nakajima, J., Matsuzawa, T., Hasegawa, A., and Zhao, D., Seismic imaging of arc magma and fluids under the central part of northeastern Japan, *Tectonophysics*, 2001, vol. 341, no. 1–4, pp. 1–17.
- Ozerov, A.Yu., The evolution of high-alumina basalts of the Klyuchevskoy volcano, Kamchatka, Russia, based on microprobe analyses of mineral inclusions, *J. Volcanol. Geotherm. Res.*, 2000, vol. 95, pp. 65–79.
- Pagli, C. and Sigmundsson, F., Will present day glacier retreat increase volcanic activity? Stress induced by recent

- glacier retreat and its effect on magmatism at the Vatnajökull ice cap, Iceland, *Geophys. Res. Lett.*, 2008, vol. 35, no. 9, p. L09304.  
<https://doi.org/10.1029/2008GL033510>
- Pan, V., Holloway, J.R., and Hervig, R.L., The pressure and temperature dependence of carbon dioxide solubility in tholeiitic basalt melts, *Geochim. Cosmochim. Acta*, 1991, vol. 55, no. 6, pp. 1587–1595.
- Paterson, M.S. and Wong, T.-F., *Brittle-ductile transition, Experimental Rock Deformation—the Brittle Field*, 2nd Ed., Berlin–Heidelberg–New York: Springer-Verlag, 2005, pp. 211–237.
- Plechov, P.Yu., Shishkina, T.A., Ermakov, V.A., and Portnyagin, M.V., Formation conditions of allivalites, olivine-anorthite crystal enclaves, in the volcanics of the Kuril-Kamchatka Arc, *Petrology*, 2008, vol. 16, no. 3.
- Ponomareva, V., Portnyagin, M., Derkachev, A., Pendea, I.F., Bourgeois, J., Reimer, P.J., and Nurnberg, D., Early Holocene M-6 explosive eruption from Plosky volcanic massif (Kamchatka) and its tephra as a link between terrestrial and marine paleoenvironmental records, *Int. J. Earth Sci.*, 2013, vol. 102, pp. 1673–1699.
- Portnyagin, M., Mironov, N., Botcharnikov, R., Gurenko, A., Almeev, R.R., Luft, C., and Holtz, F., Dehydration of melt inclusions in olivine and implications for the origin of silica-undersaturated island-arc melts, *Earth Planet. Sci. Lett.*, 2019, vol. 517, pp. 95–105.
- Putirka, K.D., Thermometers and barometers for volcanic systems, *Rev. Mineral. Geochem.*, 2008, vol. 69, no. 1, pp. 61–120.
- Putnis, A. and Austrheim, H., Fluid-induced processes: metasomatism and metamorphism, *Geofluids*, 2010, vol. 10, nos. 1–2, pp. 254–269.  
<https://doi.org/10.1111/j.1468-8123.2010.00285.x>
- Safonov, O.G., Butvina, V.G., Limanov, E.V., and Kosova, S.A., Mineral indicators of reactions involving fluid salt components in the deep lithosphere, *Petrology*, 2019, vol. 27, no. 5, pp. 489–515.
- Schmeling, H., Numerical models on the influence of partial melt on elastic, anelastic and electric properties of rocks. Part I: elasticity and anelasticity, *Phys. Earth Planet. Inter.*, 1985, vol. 41, no. 1, pp. 34–57.
- Schuler, J., Greenfield, T., White, R.S., Roecker, S.W., Brandsdóttir, B., Stock, J.M., Tarasiewicz, J., Martens, H.R., and Pugh, D., Seismic imaging of the shallow crust beneath the Krafla central volcano, NE Iceland, *J. Geophys. Res.*, 2015, vol. 120, pp. 7156–7173.
- Shishkina, T.A., Botcharnikov, R.E., Holtz, F., Almeev, R.R., and Portnyagin, M.V., Solubility of H<sub>2</sub>O- and CO<sub>2</sub>-bearing fluids in tholeiitic basalts at pressures up to 500 MPa, *Chem. Geol.*, 2010, vol. 277, no. 1–2, pp. 115–125.
- de Silva, S.L. and Gosnold, W.D., Episodic construction of batholiths: Insights from the spatiotemporal development of an ignimbrite flare-up, *J. Volcanol. Geotherm. Res.*, 2007, vol. 167, nos. 1–4, pp. 320–335.
- Simakin, A.G. and Bindeman, I.N., Convective melting and water behavior around magmatic–hydrothermal transition: numerical modeling with application to Krafla Volcano, Iceland, *J. Petrol.*, 2022, vol. 63, pp. 1–22.
- Simakin, A. and Ghassemi, A., A visco-poroelastic model with strain-history dependent rheology: application to geomechanics, *Gulf Rocks, 2004, the 6th North America Rock Mechanics Symposium (NARMS)*, OnePetro, 2004.
- Simakin, A.G. and Shaposhnikova, O.Y., Novel amphibole geobarometer for high-magnesium andesite and basalt magmas, *Petrology*, 2017, vol. 25, no. 2, pp. 226.
- Simakin, A.G. and Murav'ev, Y.D., The relationship between glaciation and volcanism: Numerical simulation and the Holocene volcanism in Kamchatka, *J. Volcanol. Seismol.*, 2017, vol. 11, pp. 187–205.
- Simakin, A., Salova, T., Devyatova, V., and Zelensky, M., Reduced carbonic fluid and possible nature of high-K magmas of Tolbachik, *J. Volcanol. Geotherm. Res.*, 2015, vol. 307, pp. 210–221.
- Simakin, A.G., Devyatova, V.N., Salova, T.P., and Shaposhnikova, O.Y., Experimental study of amphibole crystallization from the highly magnesian melt of Shiveluch Volcano, Kamchatka, *Petrology*, 2019, vol. 27, pp. 442–459.  
<https://doi.org/10.1134/S0869591119050072>
- Takei, Y., Effect of pore geometry on VP/VS: From equilibrium geometry to crack, *Journal of Geophysical Research: Solid Earth*, 2002, vol. 107, no. B2 pp. ECV 6-1–ECV 6-12.  
<https://doi.org/10.1029/2001JB000522>
- Torok, K., Degic, J., Szep, A., and Marosi, G., Reduced carbonic fluids in mafic granulite xenoliths from the Bakony–Balaton Highland Volcanic Field, W-Hungary, *Chemical Geology*, 2005, vol. 223, nos. 1–3, pp. 93–108.
- Wannamaker, P.E., Caldwell, T.G., Jiracek, G.R., Maris, V., Hill, G.J., Ogawa, Y., Bibby, H.M., Bennie, S.L., and Heise, W., Fluid and deformation regime of an advancing subduction system at Marlborough, New Zealand, *Nature*, 2009, vol. 460, no. 7256, pp. 733–736.  
<https://doi.org/10.1038/nature08204>
- Wilshire, H.G., Pike, J.E.N., Meyer, C.E., and Schwarzman, E.C., Amphibole-rich veins in lherzolite xenoliths, Dish Hill and Deadman Lake, California, *Am. J. Sci.*, 1980, vol. 280, pp. 576–593.
- Wu, T.T., The effect of inclusion shape on the elastic moduli of a two-phase material, *Int. J. Solids Struct.*, 1966, vol. 2, no. 1, pp. 1–8.
- Yardley, B.W.D., The role of water in the evolution of the continental crust, *J. Geol. Soc.*, 2009, vol. 166, no. 4, pp. 585–600.
- Yardley, B.W.D. and Valley, J.W., The petrologic case for a dry lower crust, *J. Geophys. Res.: Solid Earth*, 1997, vol. 102, no. B6, pp. 12173–12185.
- Zelenski, M., Kamenetsky, V.S., Nekrylov, N., and Kon-tonikas-Charos, A., High sulfur in primitive arc magmas, its origin and implications, *Minerals*, 2021, vol. 12, no. 1, p. 37.  
<https://doi.org/10.3390/min12010037>
- Zencher, F., Bonafede, M., and Stefansson, R., Near-lithostatic pore pressure at seismogenic depths: a thermo-poroelastic model, *Geophys. J. Int.*, 2006, vol. 166, no. 3, pp. 1318–1334.  
<https://doi.org/10.1111/j.1365-246X.2006.03069.x>